Evidence for decreasing South Asian summer monsoon in the past 160 years from varved sediment in Lake Xinluhai, Tibetan Plateau

Guoqiang Chu,[1] Qing Sun,[2] Ke Yang,[3] Aiguo Li,[3] Xiaohan Yu,[3] Tao Xu,[2] Fen Yan,[3] Hua Wang,[3] Meimei Liu,[2] Xiaohua Wang,[1] Manman Xie,[1] Yuan Lin,[2] and Qiang Liu[1]

Received 11 May 2010; revised 29 September 2010; accepted 29 October 2010; published 26 January 2011.

[1] We report glacial varves in the sediment of Lake Xinluhai, Tibetan Plateau. Independent data of ^{137}Cs and ^{210}Pb indicate that these are annually deposited varves. Varves appear as rhythmic units of light-colored silt layer capped by a dark clay layer under microscope. Varve thickness in Lake Xinluhai is sensitive to precipitation because sediment accumulation is strongly affected by monsoon rainfall in the area. A general decreasing trend can be observed in the varve thickness over the past 160 years. Spectral analyses of the varve record are dominated by cycles which are similar to ENSO periodicities. It implies that the decreasing trend of the South Asia monsoon may be linking with ENSO. Spatially, the decreasing trend can be observed across different proxy records in the south of the Tibetan Plateau. Although arguments still remain for the dynamic mechanisms and spatial rainfall difference, the South Asian summer monsoon could be weakened due to rising temperatures.

Citation: Chu, G., et al. (2011), Evidence for decreasing South Asian summer monsoon in the past 160 years from varved sediment in Lake Xinluhai, Tibetan Plateau, *J. Geophys. Res.*, *116*, D02116, doi:10.1029/2010JD014454.

1. Introduction

[2] The Tibetan Plateau covers an area of 57, 000 km^2, and plays a critical role not only on the regional climate but also on the global climate for its topographic feature and sensible heat flux [*Ruddiman and Kutzbach*, 1989; *Thompson et al.*, 2000; *Yao et al.*, 2007; *Wang et al.*, 2007]. Moreover, the Tibetan Plateau has the largest storage of ice outside the polar region, and acts as the "Water Tower of Asia" from where the Asian large rivers have their source. Therefore, it is important to study the variability of precipitation in this region. Although previous work has been done on paleoclimatic changes in the region, little is known about monsoon precipitation on the annual to century time scales on the Tibetan Plateau [*Duan et al.*, 2006]. One of the reasons for this gap in our knowledge is that the instrumental record on the Tibetan Plateau is only available for the last few decades and from a few locations, providing a very limited perspective on climate variability in the region. Ice cores provide excellent records of paleoclimatic change [*Yao et al.*, 1996; *Thompson et al.*, 2000; *Duan et al.*, 2006], but they are only available from a few locations, and there are some problems for interpretation [*Fisher and Koerner*, 1994; *Koerner*, 1997; *Bräuning*, 2006; *Kehrwald et al.*, 2008].

[3] Annually laminated sediments have been recognized at widespread geographic locations [*O'Sullivan*, 1983; *Overpeck*, 1996; *Lamoureux and Bradley*, 1996; *Smith et al.*, 2004]. However, only a few laminated sediments have been found in Asia [*Kawakami et al.*, 2004; *Kato et al.*, 2004; *Mingram et al.*, 2004; *Nakagawa et al.*, 2005; *Zhou et al.*, 2007; *Chu et al.*, 2008]. Glacial varves are annually laminated sediments that are commonly found in proglacial lakes in the Arctic and in some high mountains or high-latitude regions [e.g., *Hardy et al.*, 1996; *Gajewski et al.*, 1997; *Moore et al.*, 2001; *Lamoureux and Gilbert*, 2004; *Sun et al.*, 2006; *Loso*, 2009]. They provide detailed climate information and an inherent annual chronology for high-resolution paleoclimatic reconstruction in the Arctic and in high mountains regions.

[4] Here, we report glacial varves in Lake Xinluhai, Tibetan Plateau. We compare our results from varved sediments with multiple records derived from different proxies to gain an overall view of the regional climatic variations. Such comparison is useful as it permits to evaluate and verify the sensitivities of the different proxies [*Mann et al.*, 1999; *Lotter*, 2003; *Hodder et al.*, 2007; *Tomkins et al.*, 2008].

2. Study Site

[5] Lake Xinluhai (Yulonglacuo in Tibetan, 31° 49′N, 99° 06′E) is located in the east of the Tibetan Plateau (Figure 1a). The elevation of Lake Xinluhai is 4020 m above sea level.

[1]Key Laboratory of Cenozoic Geology and Environment, Institute of Geology and Geophysics, Chinese Academy of Sciences, Beijing, China.
[2]National Research Center of Geoanalysis, Beijing, China.
[3]Shanghai Synchrotron Radiation Facility, Shanghai Institute of Applied Physics, Chinese Academy of Sciences, Shanghai, China.

0148-0227/11/2010JD014454

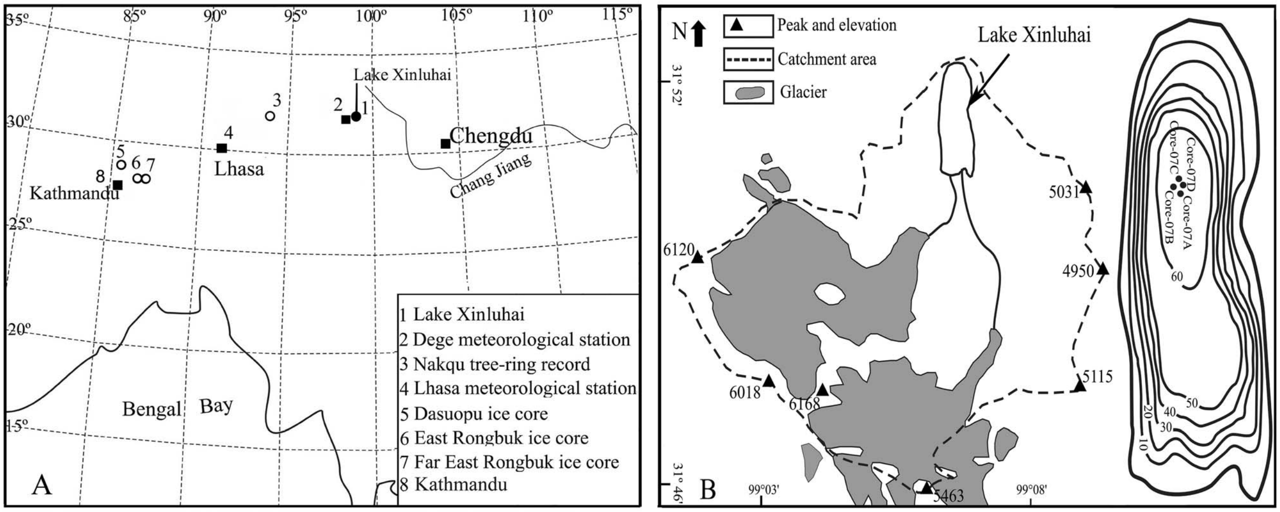

Figure 1. (a) Location of Lake Xinluhai, meteorological station, and previous records in the adjacent region. (b) Map of Lake Xinluhai study site showing the catchment outline and glacier. Right shows bathymetric map and coring sites.

The lake was dammed by frontal moraines formed after the late glacial. The lake has a surface area of 3.3 km^2, a catchment area of 75 km^2, and a maximum depth of 65 m (Figure 1b). In the south of the lake catchment, two glaciers extend from elevation of 6000 m down to 4200 m. The mainstreams enter the southern end of the lake and create a delta zone.

[6] The climate of the study region is strongly influenced by the South Asian monsoon. In summer, low pressure over the plateau induces moist and warm air masses from the Indian Ocean to the Tibetan Plateau. Most of the annual precipitation falls during the summer monsoon season. The mean annual precipitation is about 620 mm. The mean annual air temperature of the area is ca. 6.6°C. The catchment is snow covered for more than 6 months per year. The lake is ice-covered from the end of September to late March.

3. Methods

3.1. Sediment Coring

[7] In August 2007, four sediment cores were recovered from Xinluhai Lake using a gravity corer (with hammer) developed at the Institute of Geology and Geophysics, Chinese Academy of Sciences. The coring sites are shown in Figure 1b. The lengths of the cores are 46 cm (Core-07A), 55 cm (Core-07B), 86 cm (Core-07C) and 11 cm (Core-07D), respectively. Core-07D was carefully operated and allowed to slowly penetrate the sediment by gravity for the purpose of recovering a complete and undisturbed record of the uppermost sediments. Core-07D was split and photographed in the field. The other cores were sealed and transported upright back to the laboratory. In the lab, the cores were dried further by inserting paper towels before the cores were split open, photographed and sampled.

3.2. Varve Counting

[8] Sediment slabs (65 × 20 × 10 mm) were taken from the core using aluminum trays. The sediment slabs overlapped each other by 1.5 cm. The slabs were shock-freezed using liquid nitrogen, and then vacuum-dried [*Lamoureux*, 1994].

[9] The freeze-dried slabs were vacuum-penetrated with a low-viscosity synthetic resin (WSR618) in a vacuum glass tank. This process was repeated several times until the slab was well penetrated by the synthetic resin. The slabs were manufactured into thin sections.

[10] These thin sections were microscopically examined for sedimentary laminations under a stereoscopic microscope with polarized light. The boundary of varves were observed and marked with a pen in the thin sections under a stereoscopic microscope with polarized light (dark field). The marked thin sections were scanned at 2400 dpi on a Canoscan Lide 90 scanner, and combined as a stratigraphical profile in Adobe Photoshop. The combined stratigraphical profile was loaded as a base map in the program Surfer 7.0 (Golden Software). The marked varves were manually digitized along three parallel profiles using the measuring tools of the Surfer program. The data was saved as a data file, and converted the digitized data to varve thickness.

3.3. Radiometric Dating

[11] Core-07B was sampled at 0.5 cm interval. The freeze-dried samples were used for radionuclide measurement at the Institute of Geology and Geophysics, Chinese Academy of Sciences. Activity measurements of ^{137}Cs, ^{210}Pb and ^{226}Ra were carried out by gamma spectrometry using a low-background well-type germanium detector (EGPC 100P-15R). Each sample was packed in a 15 mm polyethylene tube for 3 weeks of storage in sealed containers to allow radioactive equilibration [*Hamilton et al.* 1994]. ^{210}Pb total was determined by gamma spectrometry via its energy at 46.5 keV. The short-lived ^{226}Ra daughter nuclides ^{214}Pb (241.9, 295.2 and 351.9 keV) and ^{214}Bi (609.3 keV) were measured to determine supported ^{210}Pb for the calculation of unsupported ^{210}Pb. ^{137}Cs was measured by its emissions at 662 keV. Radiometric dates were calculated from the ^{210}Pb records using the CRS model [*Appleby et al.*, 1986].

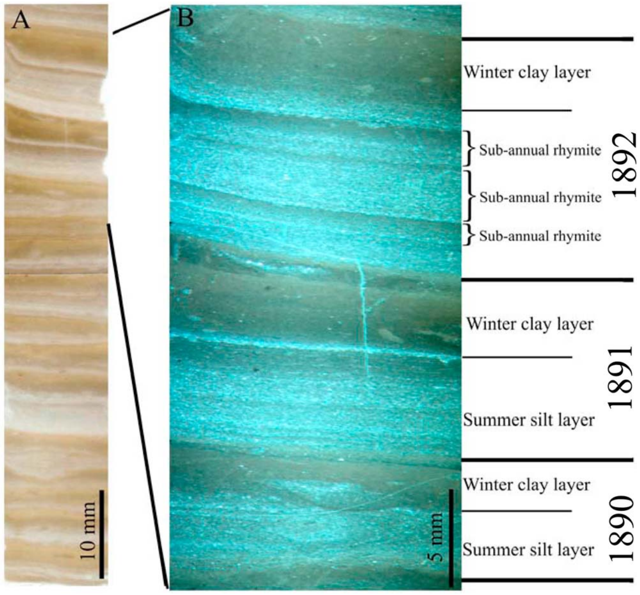

Figure 2. Photographs of varves. (a) Scanner photo of thin section from Core-07C (Tine section XLC-9: depth: 40.0–46.5 cm). (b) Microphotographs under a stereoscopic microscope (with polarized and transmitted light). Varves appear as couplets of light-silt layer and dark-clay layer. The silts grade upward into fine clay, then the clay layer sharply contacts with the silt layer of the next year. Some rhythmites can be found within the silt layer.

3.4. Synchrotron Radiation X-Ray Fluorescence Analyses

[12] Synchrotron radiation X-ray fluorescence (SRXRF) measurements were performed at the Hard X-ray beamline BL15U of Shanghai Synchrotron Radiation Facility (SSRF). Sediment slabs (60 × 10 × 10 mm) were cut from another half core using aluminum trays. The sediment slabs were fixed at a 7-axis sample stage, which was driven by step motors. The beam size is 80 × 80 μm. A Si (Li) detector was used to collect the XRF signal from samples with real time of 20s. Data were processed by using program AXIL and elemental (Ti, Ga, Rb, Sr, Ca and Zr) concentrations were obtained by comparing the elemental XRF intensity of the sample with that of the standard sample.

3.5. Other Analyses

[13] The cores were sampled at 0.5 cm interval for physical and chemical analyses. The samples were freeze-dried to determine water content and dry bulk density. Magnetic susceptibility was measured with a Bartington MS Meter. Grain size was analyzed by a laser size analyzer (Fritsch, Analysette-22). The concentrations of organic carbon and total nitrogen for selected samples were determined using a CHNS elemental analyzer (PE2400 Series CHNS/O Analyzer). The concentration of organic carbon is lees than 1.0% from four selected samples. We do not present organic carbon and total nitrogen data since the precision of the method was 0.5% and 1.0% for organic carbon and total nitrogen, respectively. We checked the thin section. There are no any diatoms and stomatocysts in the sediments.

4. Result and Discussion

4.1. Varves and Radiometric Dating

[14] Initial inspection of the fresh split surface of the cores revealed millimeter- to centimeter-scale, light- and dark-colored laminate couplets. In thin section, laminae appear as light-colored layer and dark-colored layer (clay cap) (Figure 2). This varve formation is the classic mode reported in many lakes in the Arctic and other glaciated areas [*Lamoureux and Bradley*, 1996; *Moore et al.*, 2001; *Francus et al.*, 2008; *Menounos and Clague*, 2008]. The light-colored layer is composed mainly of silt, with a gradual textural transition to the dark-colored layer. It is interpreted as the product of high sediment inflow during summer. In some cases, two or more subannual rhythmites (subannual laminae) can be observed in one varve year (Figure 2). Subannual rhythmites are normally grained into a thin fine silt-clay layer, and have a sharp contact with the overlying silt layer. It has been suggested that these sub-rhythmites might be due to high flow into lake (fast snowmelting, flood events) [*Schiefer et al.*, 2006; *Sun et al.*, 2006; *Menounos and Clague*, 2008]. The dark-colored layer is composed mainly of clay, with a sharply boundary in the overlying layer. The clay layer is deposited during the winter in which suspended clay could be deposited in a still water environment under ice-cover condition.

[15] There are two reworked layers in the sediment cores. The first reworked layer, laminated planar microbeddings, was only observed in Core-07B (21.5–25.5 cm) (Figure 3). This structure suggests that the sedimentation process was an alternance of uniform sheet flows along the bottom and deposition in still water. It could have been caused by the overloading of sediment on the slopes of the lake basin. Based on the comparing with other cores, this reworked layer might not cause erosion under sedimentary sequence (Figure 3). Second reworked layer, turbidite deposit with graded sequence, is in the bottom of Core-07C (68.5–84.5 cm) (Figure S1).[1] This structure suggests that sediment was transported by both traction load and suspension. Stratigraphically, three cores can be finely correlated.

[16] Independent data of ^{137}Cs and ^{210}Pb activities were used to verify the varve chronology in Core-07B. Figure 4a shows ^{137}Cs and unsupported ^{210}Pb activities in Core-07B. The ^{137}Cs activity is near zero below the depth of 14.5cm in Core-07B, and indicates that this horizon matches with the onset of large-scale nuclear weapons testing in the early 1950s (Figure 4). The highest ^{137}Cs (7.3 dpm/g) occurred at a depth of 10. Twenty-five cm, and is assumed to correlate to the 1963 maximum of emission due to nuclear bomb testing (Figure 4). Although the core was sampled at 0.5 cm intervals, the ^{137}Cs profile does not show the Chernobyl event. Either this event did not leave a strong signal in the studied region or is undistinguishable due to low ^{137}Cs activities. Figure 4 shows the Pb-CRS model ages, ^{137}Cs horizon and varve chronology. Although the good agreement between the varve counts and 1963 highest ^{137}Cs value, the Pb CRS

[1]Auxiliary materials are available with the HTML. doi:10.1029/2010JD014454.

Figure 3. Scanner photos of thin sections showing a reworked layer. Microlaminated bedding, a reworked layer, is only observed in Core-07B (first column). In the second column, the microlaminated bedding was cut for comparing with other cores. The depths for AD 1941 in Core-07A, Core-07B, and Core-07C are 19.1, 18.6, and 20.2 cm, respectively. The depths for AD 1927 in Core-07A, Core-07B, and Core-07C are 25.8, 24.9, and 26.6 cm, respectively.

model ages differ from the varve counts in the low part of the core. It could be relate to low levels of unsupported ^{210}Pb in the sediments, and large variations of accumulation rates as suggested by *Lamoureux and Gilbert* [2004]. High sedimentation rate may be an important reason for low levels of unsupported ^{210}Pb since it could dilute ^{210}Pb signal.

4.2. Sediment Physical Properties

[17] Figure 5 shows down-core variations in water content, bulk density, magnetic susceptibility and median grain size. The sediments consist of fine grain size ranging from clay to fine sand. Median grain size ranges from 3.0 μm to 8.8 μm with a mean value of 5.4 μm in the sediments. Coarse particles (>63 μm) are less than 1%. It is similar with typical varved sediments in the Arctic [*Sun et al.*, 2006; *Francus et al.*, 2008].

[18] Bulk density is from 0.5 g/cm^3 to 0.9 g/cm^3 with a mean value of 0.64 g/cm^3 (Figure 5). The constant bulk density with depth suggests that sediment compaction is not significant. The bulk density appears to correlate with the variation of median grain size. Magnetic susceptibility values vary between 4×10^{-8} and 12×10^{-8} (m^3/kg) in the profile. The variations of magnetic susceptibility negatively correlate with grain size (Pearson coefficient $r = -0.54$, $p < 0.001$) (Figure 5). It may suggest that the finer fraction contributes more to magnetic susceptibility in the sediments.

4.3. Extracting the Climate Signal From Varved Sediment

[19] The thickness of varves in Lake Xinluhai varies between 1.0 mm and 11.0 mm with a mean value of 3.9 mm. Varve thickness in Core-07D was calibrated by multiplying a factor of 0.6 since the water content was very high in the core (Core-07D was open in the field). After the calibration for Core-07D, the varve thickness in AD 1988 (a marker layer) in the Core07-A, B, C and D is 8.75, 8.25, 8.39 and 8.49, respectively. Figure 6 shows varve thickness in the sediment cores. There is a close relationship among four cores, which indicates that sediment deposition in the lake is stable.

[20] Previous studies have demonstrated that varve thickness could be controlled by various factors, such as summer temperature [*Leemann and Niessen*, 1994; *Hughen et al.*, 2000; *Moore et al.*, 2001; *Loso et al.*, 2006, *Tomkins et al.*, 2008], snowmelt runoff [*Leemann and Niessen*, 1994] and hydroclimatic parameter [*Lamoureux and Gilbert*, 2004; *Desloges and Gilbert*, 1994; *Sander et al.*, 2002; *Menounos et al.*, 2005; *Hodder et al.*, 2007; *Cockburn and Lamoureux*, 2007]. The relationship between varve formation and climatic factors is very complex. For example, summer temperature may play an important role for varve thickness in very cold regions or polar desert areas since temperature is first factor for melting ice and snow [e.g., *Hughen et al.*, 2000; *Moore et al.*, 2001; *Sun et al.*, 2006]. By contrast, precipitation may play an important role in the area with high precipitation. Intense rainfall events during snow/ice-free summer months can produce brief periods of high-sediment loads, and therefore thicker than normal laminations [*Hardy et al.*, 1996; *Francus et al.*, 2002]. To assess different climatic factors in the variation of varve thickness, we used instrumental data from the nearest weather station (Figure 1) to test the relationship between varve thickness and meteorological data (monthly temperature and precipitation).

[21] In order to compare varve thickness with meteorological data, the following equation was used to standardize the data [*Zolitschka*, 1996; *Boës and Fagel*, 2008]:

$$Z = (X - U)/S$$

where Z is the standardized varve thickness, X is the measured varve thickness, U is the mean value of all varve thickness data, and S is the standard deviation of varve thickness. The same equation was also used to standardize the instrumental climate data. The varve thickness in Lake Xinluhai are positively correlated with spring (March, April,

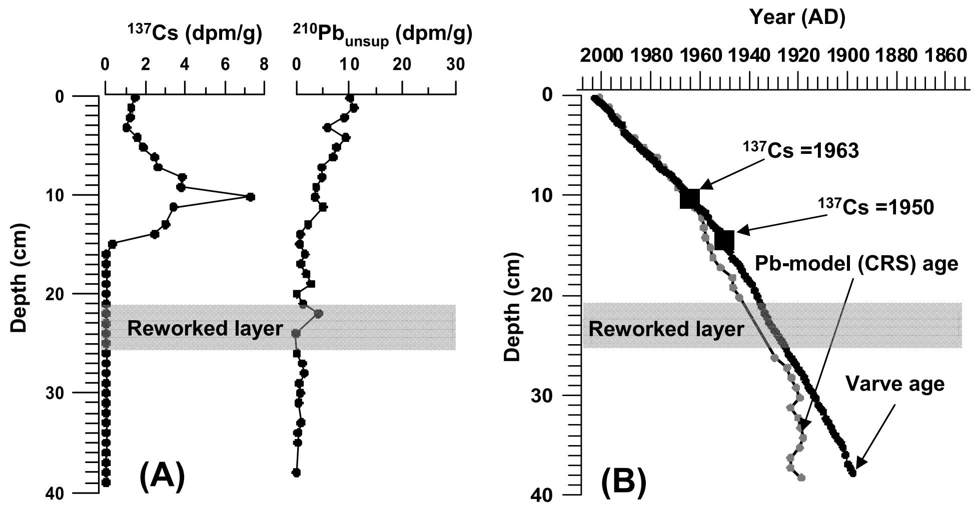

Figure 4. (a) The ^{137}Cs and unsupported ^{210}Pb activity versus depth in Core-07B. (b) Varve ages and Pb-model (CRS) ages versus depth in Core-07B. The reworked layer in Core-07B was removed.

May) precipitation (Pearson coefficient: r = 0.51, n = 49, $p < 0.005$) in Dege station (Table 1).The varve thickness does show significant correlation with temperature data set (Table 1). The variations of varve thickness largely depend on available material transported by runoff [*Desloges and Gilbert*, 1994; *Hodder et al.*, 2007]. High precipitation could yield more strong runoff and sedimentation to Lake Xinluhai. In addition, spring rainfall may be favorable for snowmelt runoff and sediment delivery [*Forbes and Lamoureux*, 2005].

[22] Synchrotron radiation X-ray fluorescence (SRXRF) measurement provides an approach to continuous nonde-

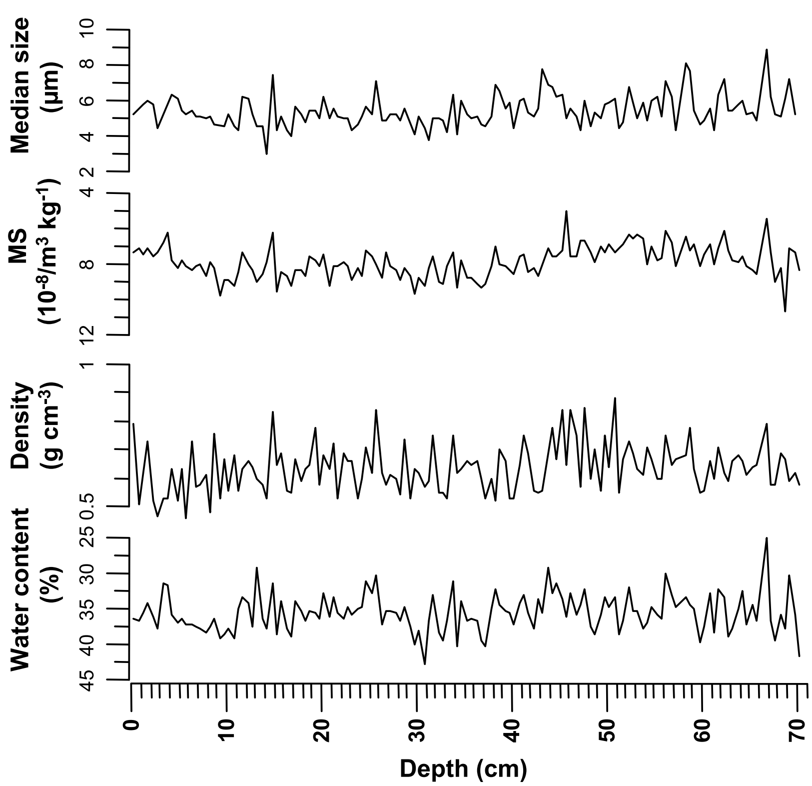

Figure 5. Down-core variations in water content, bulk density, magnetic susceptibility (MS) and median grain size. Note: Water content, bulk density, magnetic susceptibility, and median grain size were analyzed from combined samples in Core-07B (0–45 cm) and Core-07C (41–67 cm).

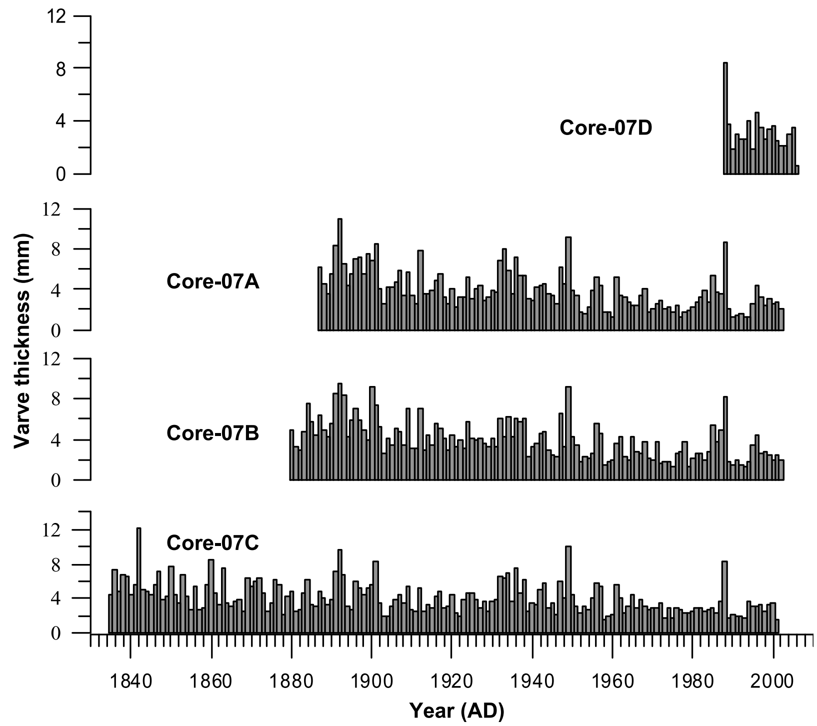

Figure 6. Variation of varve thickness in the sediment cores.

structive analyze elements under a sharp synchrotron beam combined with measurements of the X-ray fluorescence [*Daryin et al.*, 2005; *Kalugin et al.*, 2005, 2007; *Goldberg et al.*, 2007]. Figure 7 shows an example of Synchrotron radiation X-ray fluorescence (SRXRF) analyses. Generally, Ti is higher in the summer silt layer, and lower in the winter clay layer (Figure 7). It implicates that grain size is an important factor to regulate elements in the lake sediments, especially on the seasonal scale. In contrast, Rb/Sr ratio seems not to be regulated by grain size significantly.

[23] On the longer time scale, however, previous research researches proposed that Ti concentration is an indicator of physical weathering and precipitation [*Dean et al.*, 2004; *Selvaraj et al.*, 2007], and Rb/Sr ratio is an indicator of chemical weathering, and low Rb/Sr values indicating warm and humid climate [*Goldberg et al.*, 2007; *Daryin et al.*, 2005; *Kalugin et al.*, 2005, 2007; *Jin et al.*, 2006]. Stratigraphically, the variations of Titanium show a weak decrease trend. A broadly similar variation can be observed in the varve thickness and Ti concentration over the past 160 years (Pearson coefficient, $r = 0.22$, $p < 0.001$ for Ti concentration and varve thickness) (Figure 8). It implicates that increase of Ti may be response to more detrital input from the catchment basin for high precipitation/runoff. Rb/Sr ratio shows a negative trend against varve thickness (Pearson coefficient, $r = 0.14$, $p < 0.001$ for Rb/Sr ratio and varve thickness) (Figure 8). The elements in the lake sediments vary mainly depending on particle size, precipitation, temperature, and water chemistry. The Rb/Sr data in this study suggested that

Table 1. Correlations Between Standardized Instrumental Climate Data and Varve Thickness From Lake Xinluhai[a]

Climate Parameters	Jan	Feb	Mar	Apr	May	Jun	Jul	Aug	Sep	Oct	Nov	Dec	Spring	Annual
Precipitation in Dege station	0.08	−0.04	0.62	0.26	0.29	−0.20	−0.02	0.07	0.19	−0.15	0.07	−0.06	**0.51**	0.15
Temperature in Dege station	0.14	0.13	−0.05	−0.19	−0.23	0.06	0.08	−0.02	0.03	0.12	−0.14	−0.14	−0.22	−0.02
Indian Ocean air temperature	0.12	0.10	0.10	0.04	0.02	018	0.13	0.05	0.03	0.01	0.05	0.12	0.05	0.00
PDO index	0.01	−0.03	0.11	0.10	0.01	0.06	−0.02	−0.11	−0.05	−0.01	0.04	0.03	0.08	0.02
AO index	0.14	−0.18	−0.12	0.09	−0.05	−0.06	−0.03	0.06	0.05	0.12	−0.08	−0.02	−0.06	−0.03
Niño 3	−0.27	−0.43	−0.32	−0.44	−0.29	0.12	−0.40	−0.39	**−0.59**	−0.39	−0.40	**−0.58**	**−0.61**	**−0.54**
Niño 3.4	−0.27	−0.26	−0.27	−0.27	−0.25	−0.16	−0.12	−0.06	−0.11	−0.12	−0.11	−0.08	−0.22	−0.28
SOI Indonesia	−0.11	−0.17	0.12	−0.02	0.05	0.13	0.05	0.13	0.02	0.05	−0.07	0.00	0.05	−0.03
SOI equatorial eastern Pacific	0.12	−0.12	0.20	0.10	0.02	0.07	0.08	0.06	0.04	0.07	0.18	0.02	0.08	0.06

[a]Monthly precipitation and temperature (1957–2005) are from China Meteorological Data Sharing Service System. Monthly Indian Ocean air temperature anomalies (1835–2003) and indices of the AO (1900–2002), Niño 3 (1950–2005), Niño 3.4 (1950–2005), the SOI Insonsia (1950–2005), and SOI equatorial eastern Pacific (1950–2005) are extracted from http://jisao.washington.edu/data/indiansat. Indices of the PDO (1900–2005) are from http://www.atmos.washington.edu/~mantua/abst.PDO.html. Values in bold font are from Dege Meteorological Station shown in Figure 1. The Niño 3 is sea-surface temperature in the eastern Pacific Ocean (2.5°S–2.5°N, 92.5°W–147.5°W) [*Mann et al.*, 2009]. The Niño 3.4 is sea-surface temperature in the region (5°S–5°N,170°W–120°W). Values in bold font indicate the strongest correlation.

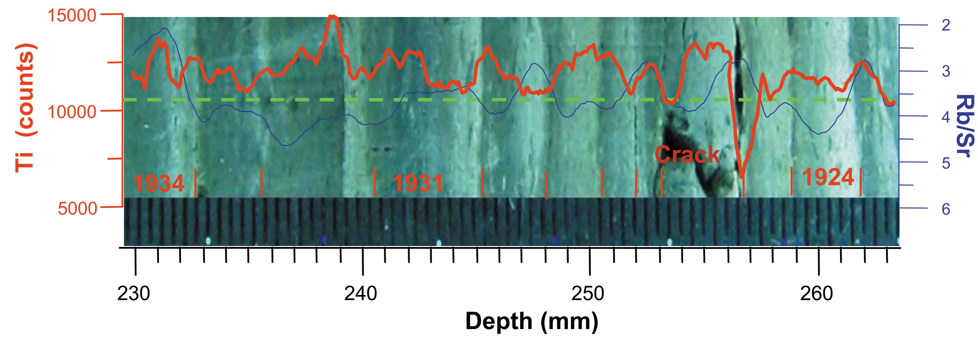

Figure 7. Synchrotron radiation X-ray fluorescence (SRXRF) analyses. Sediment slab Photo shows varves marked the boundary by red line (AD1924-1934) in Core 07-D (Depth: 23.0–26.3 cm). Red curve is Ti content. Blue curve is Rb/Sr ration.

both chemical and physical process regulate the variation over past 160 years.

4.4. Comparison of Regional Records and Physical Explanation

[24] Spatial paleoclimatic variation is useful to valuate and verify the sensitivities of different proxy records. We compare the varve data in this study with the Palmer Drought Severity Index from Nakqu tree ring records [*Wang et al.*, 2008], snow accumulation data from Dasopu ice core [*Duan et al.*, 2006] and East Rongbuk ice core [*Zhang et al.*, 2004] in the southern Tibet, and annual Kathmandu precipitation [*Cook et al.*, 2003]. Although different proxies have unique formative processes and environmental sensitivities, a similar decreasing pattern can be identified across different proxy records and different localities (Figure 9). The inherent relationship may link with the South Asian Monsoon since monsoonal air masses flowing over the Bay of Bengal pass through southern Nepal, northwestern Yunan and then penetrate into the study region.

[25] At the interannual to interdecadal time scales, the variations of the monsoon have been linked to the El Niño–Southern Oscillation (ENSO) [*Webster et al.*, 1998; *Linsley et al.*, 2000; *Gadgil et al.*, 2004; *Goswami and Xavier*, 2005; *Wang et al.*, 2008] and the Arctic Oscillation (AO) [*Zhao and Moore*, 2004; *Buermann et al.*, 2005]. Recently, *Ashfaq et al.* [2009] proposed that enhanced greenhouse forcing resulted in over all suppression of summer precipitation. Table 1 shows the correlations between varve thickness and global-hemispherical climate factors (Indian Ocean air temperature anomalies, the Arctic Oscillation (AO), Niño 3, Niño3.4, the Southern Oscillation (SOI) Insonsia, the SOI equatorial eastern Pacific and the Pacific Decadal Oscillation (PDO)). A significant negative corre-

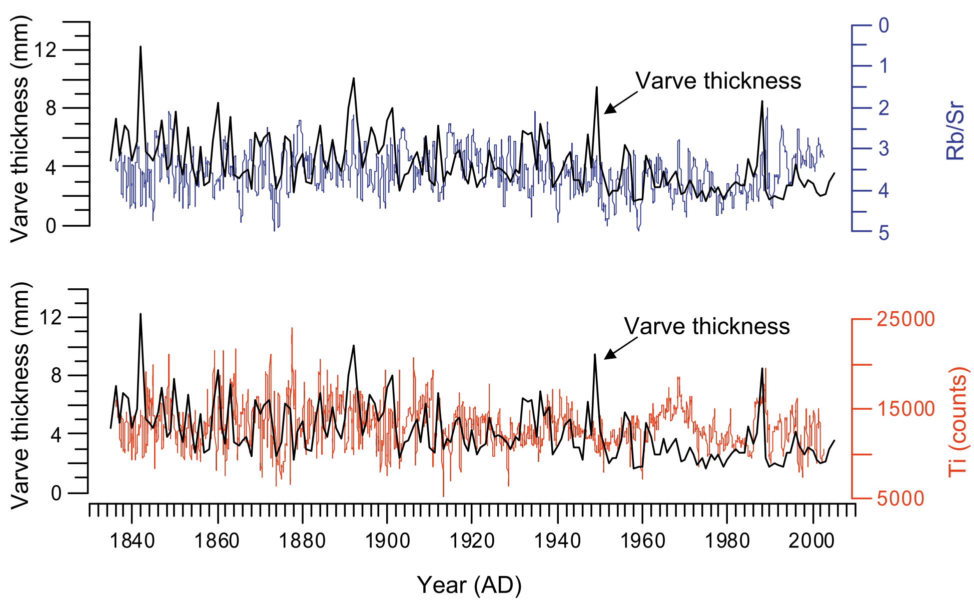

Figure 8. Comparative diagrams of the varve thickness, Ti content, and Rb/Sr ratio. According to the varve thickness in each year and the measured step (SRXRF), time scales for each SRXRF data were calculated. Ti content and Rb/Sr ratio were smoothed with 11-point running average.

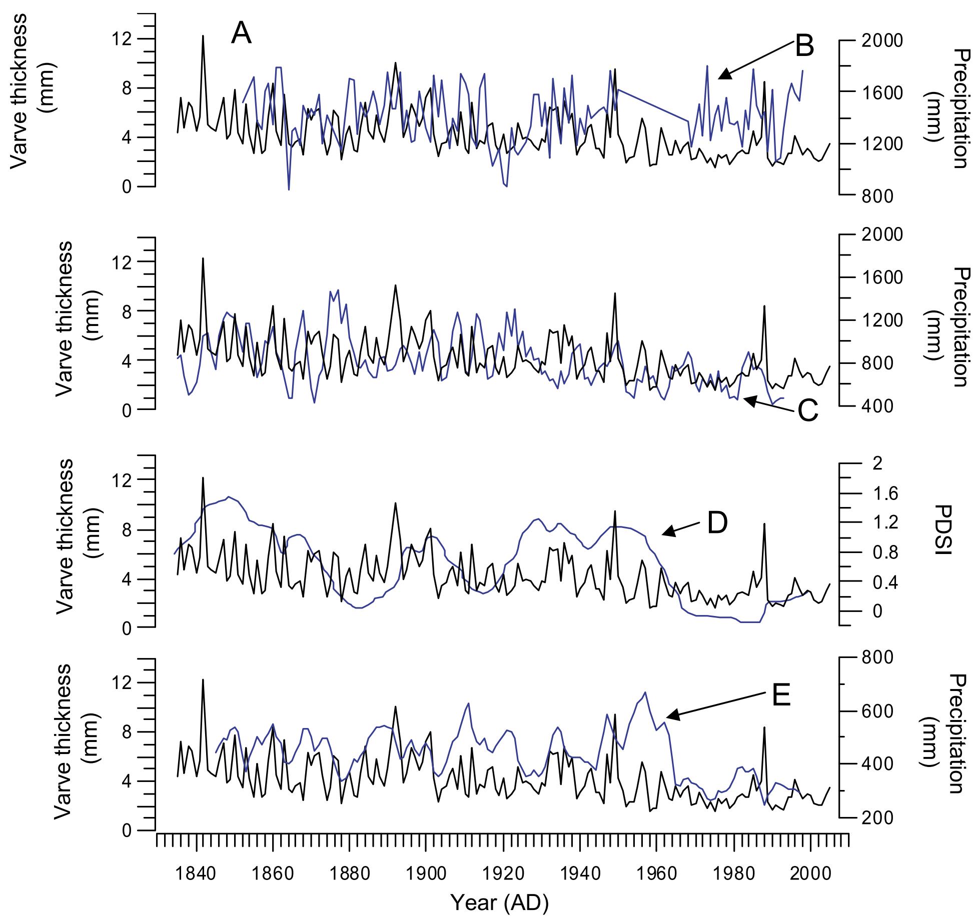

Figure 9. Comparison of the variations of varve thickness in this study, proxy data, and meteorological data in the adjacent region. Varve thickness in Lake Xinluhai (mean values from four cores) (curve A). Annual Kathmandu precipitation (curve B). (The data from 1851 to 1950 are from [*Cook et al.* 2003], and the data from 1968 to 1998 are from Kathmandu Airport.) Snow accumulation data with 3-point running average from Dasopu ice core [*Duan et al.*, 2006] (curve C). Palmer Drought Severity Index (PDSI) with 3-point running average from Nakqu in the southern Tibet [*Wang et al.*, 2008] (curve D). Snow accumulation data with 3-point running average from East Rongbuk ice core [*Zhang et al.*, 2004] (curve E). The locations of different records are shown in Figure 1.

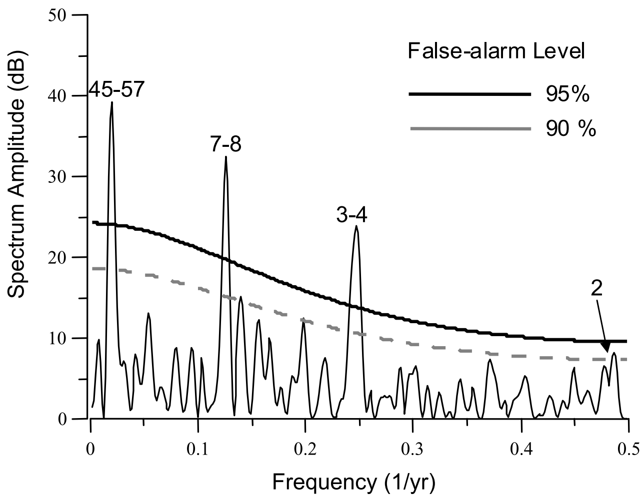

Figure 10. Spectral analysis results of the varve thickness time series. The spectra were estimated using the program REDFIT [*Schulz and Mudelsee*, 2002] with OFAC = 4 and HIFAC = 1. One thousand Monte Carlos simulations were used for the bias correction. The spectral window is a Welch I type. The red noise alternative is upper 95% χ^2 bound (smooth line) from a first-order autoregressive (AR1) process.

lation with Niño SST is shown in the Table 1. There is no significant correlation between the varve thickness and other climate parameters (Table 1).

[26] Spectral analysis shows three significant periodicities (3–4, 7–8, 45–57) at a confidence level greater than 95% in the varve thickness (Figure 10). Periodicities in the range of 3–8 years are classical ENSO periodicities [*Allan*, 2003]. However, ENSO-related multidecadal variability has not well discussed, but seen in some proxy records [*Minobe*, 1997; *MacDonald and Case*, 2005; *Fagel et al.*, 2008]. The reason for the multidecadal periodicities (45–47 years) is not clear, but could be link to solar activity or nonlinear dynamics in the ocean-atmosphere system [*MacDonald and Case*, 2005].

[27] The ENSO, a coupled atmospheric–oceanic phenomenon, is the most significant factor causing global hydroclimatic variability [*Allan*, 2003; *Shrestha and Kostaschuk*, 2005; *Fagel et al.*, 2008]. Generally, El Niño (La Niña) events cause a warming (cooling) in tropical Pacific and Indian Oceans that tends to suppress (enhance) the monsoon [*Webster*, 1995; *Torrence and Webster*, 1999; *Krishnamurthy and Goswami*, 2000]. Figure 11 shows comparison of the varve thickness in this study with the Niño 3 series [*Mann et al.*, 2009]. A decreasing trend in the varve thickness is negatively correlated with the Niño 3 index of ENSO (Figure 11). It supports the previous suggestion that the time series of Niño3 SST and Indian rainfall is negatively correlated with the interannual ENSO signal [*Torrence and Webster*, 1999]. The physical link for the decrease in the monsoon rainfall associated with the warm phases of ENSO could be due to an anomalous regional Hadley circulation with descending motion over the Indian continent and ascending motion near the equator sustained by the ascending phase of the anomalous Walker circulation in the equatorial Indian Ocean [*Krishnamurthy and Goswami*, 2000]. Although arguments still remain for the dynamic mechanisms and spatial rainfall pattern, the South Asian summer monsoon could be weakened due to rising temperatures in the past 160 years and in the future.

5. Conclusions

[28] Glacial varves are reported for the first time from Lake Xinluhai, Tibetan Plateau. By comparing the results of varve counting, thin section observations and independent radiometric data, we could demonstrate that the sedimentary record of Lake Xinluhai is annually laminated. Our result reveals that varve thickness in Lake Xinluhai is sensitive to the variations of precipitation. High precipitation could yield stronger runoff, sedimentation and Ti to Lake Xinluhai.

[29] A general decreasing trend in the varve thickness can be observed over the past 160 years. This decreasing trend can be observed in other multiple records (PDSI and snow accumulation data) in the south of Tibetan Plateau. Spectral analyses of the varve record are dominated by cycles that are similar to ENSO periodicities. It implies that the South Asia summer monsoon may be linking with ENSO. It is likely that glacial varves are being formed in many lakes on the Tibetan Plateau. Glacial varve record should therefore play an important role as a reliable high-resolution paleoclimatic proxy in this data-sparse area.

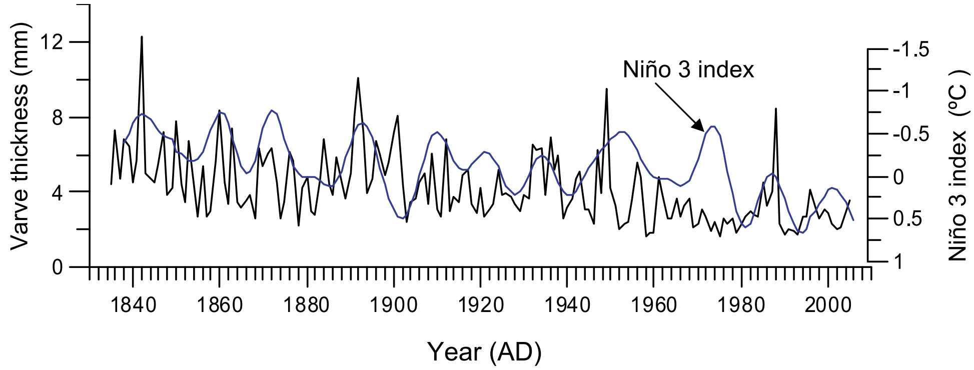

Figure 11. Comparison of the variations of varve thickness and Niño 3 index. Varve thickness is mean values from four cores. Niño 3 index is from [*Mann et al.* 2009].

[30] **Acknowledgments.** We are grateful to I. Kalugin, N. Fagel, and anonymous reviewers for their constructive comments. This study was supported by National Basic Research Program of China (973 Program, 2010CB950201) and the National Natural Science Foundation of China (grants 40571148 and 4032531002).

References

Allan, R. (2003), ENSO and climatic variability in the past 150 years, in *El Niño and the Southern Oscillation: Multiscale Variability and Global and Regional Impacts*, edited by H. Diaz and V. Markgraf, pp. 3–35, Cambridge Univ. Press, Cambridge, U. K.

Appleby, P. G., P. J. Nolan, D. W. Gifford, M. J. Godfrey, F. Oldfield, N. J. Anderson, and R. W. Battarbee (1986), ^{210}Pb dating by low background gamma counting, *Hydrobiologia*, *143*, 21–27, doi:10.1007/BF00026640.

Ashfaq, M., Y. Shi, W. W. Tung, R. J. Trapp, X. Gao, J. S. Pal, and N. S. Diffenbaugh (2009), Suppression of South Asian summer monsoon precipitation in the 21st century, *Geophys. Res. Lett.*, *36*, L01704, doi:10.1029/2008GL036500.

Boës, N., and N. Fagel (2008), Timing of the late glacial and Younger Dryas cold reversal in southern Chile varved sediments, *J. Paleolimnol.*, *39*, 267–281, doi:10.1007/s10933-007-9118-x.

Bräuning, A. (2006), Tree-ring evidence of “Little Ice Age” glacier advances in southern Tibet, *Holocene*, *16*, 369–380, doi:10.1191/0959683606hl922rp.

Buermann, W., B. Lintner, and C. Bonfils (2005), A wintertime Arctic Oscillation signature on early season Indian Ocean monsoon intensity, *J. Clim.*, *18*, 2247–2269, doi:10.1175/JCLI3377.1.

Chu, G. Q., Q. Sun, P. Rioual, A. Boltovskoy, Q. Liu, P. Q. Sun, J. T. Han, and J. Q. Liu (2008), Dinocyst microlaminations and freshwater “red tides” recorded in Lake Xiaolongwan, northeastern China, *J. Paleolimnol.*, *39*, 319–333, doi:10.1007/s10933-007-9106-1.

Cockburn, J. M. H., and S. F. Lamoureux (2007), Century-scale variability in late-summer rainfall events recorded over seven centuries in subannually laminated lacustrine sediments, White Pass, British Columbia, *Quat. Res.*, *67*, 193–203, doi:10.1016/j.yqres.2006.10.003.

Cook, E. R., P. J. Krusic, and P. D. Jones (2003), Dendroclimatic signals in long tree-ring chronologies from the Himalayas of Nepal, *Int. J. Climatol.*, *23*, 707–732, doi:10.1002/joc.911.

Daryin, A. V., I. A. Kalugin, N. V. Maksimova, L. G. Smolyaninova, and K. V. Zolotarev (2005), Use of a scanning XRF analysis on SR beams from VEPP-3 storage ring for research of core bottom sediments from Teletskoe Lake with the purpose of high resolution quantitative reconstruction of the last millennium paleoclimate, *Nucl. Instrum. Methods A*, *543*, 255–258.

Dean, W., C. Pride, and R. Thunell (2004), Geochemical cycles in sediments deposited on the slopes of the Guaymas and Carmen basins of the Gulf of California over the last 180 years, *Quat. Sci. Rev.*, *23*, 1817–1833, doi:10.1016/j.quascirev.2004.03.010.

Desloges, J. R., and R. Gilbert (1994), Sediment source and hydroclimatic inferences from glacial lake sediments: The post glacial sedimentary record of Lillooet Lake, British Columbia, *J. Hydrol.*, *159*, 375–393, doi:10.1016/0022-1694(94)90268-2.

Duan, K., T. Yao, and L. G. Thompson (2006), Response of monsoon precipitation in the Himalayas to global warming. *J. Geophys. Res.*, *111*, D19110, doi:10.1029/2006JD007084.

Fagel, N., N. Boës, and M. F. Loutre (2008), Climate oscillations evidenced by spectral analysis of southern Chilean lacustrine sediments: The assessment to ENSO over the last 600 years, *J. Paleolimnol.*, *39*, 253–266, doi:10.1007/s10933-007-9116-z.

Fisher, D. A., and R. M. Koerner (1994), Signal and noise in four ice-core records from the Agassiz Ice Cap, Ellesmere Island, Canada: Details of the last millennium for stable isotopes, melt, and solid conductivity, *Holocene*, *4*, 113–120, doi:10.1177/095968369400400201.

Forbes, A. C., and S. F. Lamoureux (2005), Climatic controls on stream flow and suspended sediment transport in three large middle arctic catchments, Boothia Peninsula, Nunavut, Canada, *Arct. Antarct. Alp. Res.*, *37*, 304–315, doi:10.1657/1523-0430(2005)037[0304:CCOSAS]2.0.CO;2.

Francus, P., R. S. Bradley, M. A. Abbott, W. Patridge, and F. Keimig (2002), Paleoclimate studies of minerogenic sediments using annually resolved textural parameters, *Geophys. Res. Lett.*, *29*(20), 1998, doi:10.1029/2002GL015082.

Francus, P., R. S. Bradley, T. Lewis, M. Abbott, M. Retelle, and J. S. Stoner (2008), Limnological and sedimentary processes at Sawtooth Lake, Canadian High Arctic, and their influence on varve formation, *J. Paleolimnol.*, *40*, 963–985, doi:10.1007/s10933-008-9210-x.

Gadgil, S., P. N. Vinayachandran, P. A. Francis, and S. Gadgil (2004), Extremes of the Indian summer monsoon rainfall, ENSO and equatorial Indian Ocean oscillation, *Geophys. Res. Lett.*, *31*, L12213, doi:10.1029/2004GL019733.

Gajewski, K., P. B. Hamilton, and R. McNeely (1997), A high resolution proxy-climate record from an arctic lake with annually laminated sediments on Devon Island, Nunavaut, Canada, *J. Paleolimnol.*, *17*, 215–225, doi:10.1023/A:1007984617675.

Goldberg, E. L., M. A. Phedorin, E. P. Chebykin, K. B. Zolotarev, and N. A. Zhuchenko (2007), Decade–centenary resolution records of climate changes in East Siberia from elements in the bottom sediments of lake Baikal for the last 150 kyr, *Nucl. Instrum. Methods A*, *575*, 193–195.

Goswami, B. N., and P. K. Xavier (2005), ENSO control on the South Asian monsoon through the length of the rainy season, *Geophys. Res. Lett.*, *32*, L18717, doi:10.1029/2005GL023216.

Hamilton, T. F., S. Ballestra, M. S. Baxter, J. Gastaud, I. Osvath, P. Parsi, P. P. Povinec, and E. M. Scott (1994), Radiometric investigations of Kara Sea sediments and preliminary radiological assessment related to dumping of radioactive wastes in the Arctic seas, *J. Environ. Radioact.*, *25*, 113–134, doi:10.1016/0265-931X(94)90011-6.

Hardy, D. R., R. S. Bradley, and B. Zolitschka (1996), The climatic signal in varved sediments from Lake C2, northern Ellesmere Island, *J. Paleolimnol.*, *16*, 227–238, doi:10.1007/BF00176938.

Hodder, K. R., R. Gilbert, and J. R. Desloges (2007), Glaciolacustrine varved sediment as an alpine hydroclimatic proxy, *J. Paleolimnol.*, *38*, 365–394, doi:10.1007/s10933-006-9083-9.

Hughen, K. A., J. T. Overpeck, and R. F. Anderson (2000), Recent warming in a 500-year paleotemperature record from varved sediments, Upper Soper Lake, Baffin Island, Canada, *Holocene*, *10*, 9–19, doi:10.1191/095968300676746202.

Jin, Z. D., J. J. Cao, J. L. Wu, and S. M. Wang (2006), A Rb/Sr record of catchment weathering response to Holocene climate change in Inner Mongolia, *Earth Surf. Process. Landforms*, *31*, 285–291.

Kalugin, I., V. Selegei, E. Goldberg, and G. Seret (2005), Rhythmic fine-grained sediment deposition in Lake Teletskoye, Altai, Siberia, in relation to regional climate change, *Quat. Int.*, *136*, 5–13, doi:10.1016/j.quaint.2004.11.003.

Kalugin, I., A. Daryin, L. Smolyaninova, A. Andreev, B. Diekmann, and O. Khlystov (2007), 800-yr-long records of annual air temperature and precipitation over southern Siberia inferred from Teletskoye Lake sediments, *Quat. Res.*, *67*, 400–410, doi:10.1016/j.yqres.2007.01.007.

Kato, M., Y. Tanimura, and H. Fukusawa (2004), Survival strategy of diatom species living on now-depositing non-glacial varves, *Quat. Int.*, *122–125*, 21–26, doi:10.1016/j.quaint.2004.02.004.

Kawakami, I., M. Matsuo, M. Kato, and H. Fukusawa (2004), Chronology and sedimentation process of varved lacustrine sediment in Lake Fukami, central Japan, *Quat. Int.*, *123–125*, 27–34, doi:10.1016/j.quaint.2004.02.005.

Kehrwald, N. M., L. G. Thompson, Y. Tandong, E. Mosley-Thompson, U. Schotterer, V. Alfimov, J. Beer, J. Eikenberg, and M. E. Davis (2008), Mass loss on Himalayan glacier endangers water resources, *Geophys. Res. Lett.*, *35*, L22503, doi:10.1029/2008GL035556.

Koerner, R. M. 1997, Some comments on climatic reconstruction from ice cores drilled in areas of high melt, *Glaciology*, *43*, 90–97.

Krishnamurthy, V., and B. N. Goswami (2000), Indian Monsoon–ENSO relationship on interdecadal times, *J. Clim.*, *13*, 579–595, doi:10.1175/1520-0442(2000)013<0579:IMEROI>2.0.CO;2.

Lamoureux, S. F. (1994), Embedding unfrozen lake sediments for thin section preparation, *J. Paleolimnol.*, *10*, 141–146, doi:10.1007/BF00682510.

Lamoureux, S. F., and R. S. Bradley (1996), A late Holocene varved sediment record of environmental change from northern Ellesmere Island, *J. Paleolimnol.*, *16*, 239–255, doi:10.1007/BF00176939.

Lamoureux, S. F., and R. Gilbert (2004), A 750-yr record of autumn snowfall and temperature variability and winter storminess recorded in the varved sediments of Bear Lake, Devon Island, Arctic Canada, *Quat. Res.*, *61*, 134–147, doi:10.1016/j.yqres.2003.11.003.

Leemann, A., and F. Niessen (1994), Varve formation and the climatic record in an Alpine proglacial lake: Calibrating annually laminated sediments against hydrological and meteorological data, *Holocene*, *4*, 1–8, doi:10.1177/095968369400400101.

Linsley, B. K., G. M. Wellington, and D. P. Schrag (2000), Decadal sea surface temperature variability in the sub-tropical South Pacific from 1726 to 1997 A. D, *Science*, *290*, 1145–1148, doi:10.1126/science.290.5494.1145.

Loso, M. G. (2009), Temperatures during the Medieval Warm Period and Little Ice Age inferred from varved proglacial lake sediments in southern Alaska, *J. Paleolimnol.*, *41*, 117–128, doi:10.1007/s10933-008-9264-9.

Loso, M. G., R. S. Anderson, S. P. Anderson, and P. J. Reimer (2006), A 1500-year record of temperature and glacial response inferred from varved Iceberg Lake, south central Alaska, *Quat. Res.*, *66*, 12–24, doi:10.1016/j.yqres.2005.11.007.

Lotter, A. F. (2003), Multi-proxy climatic reconstructions, in *Global Change in the Holocene*, edited by A. Mackay et al., pp. 373–383, Arnold Publ., London.

MacDonald, G. M., and R. A. Case (2005), Variations in the Pacific Decadal Oscillation over the past millennium, *Geophys. Res. Lett.*, *32*, L08703, doi:10.1029/2005GL022478.

Mann, M. E., R. S. Bradley, and M. K. Hughes (1999), Northern Hemisphere temperatures during the past millennium: Inferences, uncertainties, and limitations, *Geophys. Res. Lett.*, *26*, 759–762, doi:10.1029/1999GL900070.

Mann, M. E., Z. Zhang, S. Rutherford, R. S. Bradley, M. K. Hughes, D. Shindell, C. Ammann, G. Faluvegi, and F. Ni (2009), Global signatures and dynamical origins of the Little Ice Age and Medieval climate anomaly, *Science*, *326*, 1256–1260, doi:10.1126/science.1177303.

Menounos, B., and J. J. Clague (2008), Reconstructing hydro-climatic events and glacier fluctuations over the past millennium from annually laminated sediments of Cheakamus Lake, southern Coast Mountains, British Columbia, Canada, *Quat. Sci. Rev.*, *27*, 701–713, doi:10.1016/j.quascirev.2008.01.007.

Menounos, B., J. J. Clague, R. Gilbert, and O. Slaymaker (2005), Environmental reconstruction from a varve network in the southern Coast Mountains, British Columbia, Canada, *Holocene*, *15*, 1163–1171, doi:10.1191/0959683605hl888rp.

Mingram, J., J. R. M. Allen, C. Brüchmann, J. Liu, X. Luo, J. F. W. Negendank, N. Nowaczyk, and G. Schettler (2004), Maar- and crater lakes of the Long Gang Volcanic Field (N.E. China): Overview, laminated sediments, and vegetation history of the last 900 years, *Quat. Int.*, *123–125*, 135–147, doi:10.1016/j.quaint.2004.02.014.

Minobe, S. (1997), A 50–70 year climatic oscillation over the North Pacific and North America, *Geophys. Res. Lett.*, *24*, 683–686, doi:10.1029/97GL00504.

Moore, J. J., K. A. Hughen, G. H. Miller, and J. T. Overpeck (2001), Little Ice Age recorded in summer temperature reconstruction from varved sediments of Donard Lake, Baffin Island, Canada, *J. Paleolimnol.*, *25*, 503–517, doi:10.1023/A:1011181301514.

Nakagawa, T., H. Kitagawa, Y. Yasuda, P. E. Tarasov, K. Gotanda, and Y. Sawai (2005), Pollen/event stratigraphy of the varved sediment of Lake Suigetsu, central Japan from 15,701 to 10,217 yr BP (Suigetsu varve years before present): Description, interpretation, and correlation with other regions, *Quat. Sci. Rev.*, *24*, 1691–1701, doi:10.1016/j.quascirev.2004.06.022.

O'Sullivan, P. E. (1983), Annually laminated lake sediments and the study of Quaternary environmental changes: A review, *Quat. Sci. Rev.*, *1*, 245–313, doi:10.1016/0277-3791(83)90008-2.

Overpeck, J. T. (1996), Varved sediment records of recent seasonal to millennial-scale environmental variability, in *Climatic Variations and Forcing Mechanisms of the Last 2000 Years*, edited by P. D. Jones, R. S. Bradley, and J. Jouzel, pp. 479–497, Springer, Berlin.

Ruddiman, W. F., and J. E. Kutzbach (1989), Forcing of late Cenozoic Northern Hemisphere climate by plateau uplift in southern Asia and the American west, *J. Geophys. Res.*, *94*, 18,409–18,427, doi:10.1029/JD094iD15p18409.

Sander, M., L. Bengtsson, B. Holmquist, B. Wohlfarth, and I. Cato (2002), The relationship between annual varve thickness and maximum annual discharge (1909–1971), *J. Hydrol.*, *263*, 23–35, doi:10.1016/S0022-1694(02)00030-6.

Schiefer, E., B. Menounos, and O. Slaymaker (2006), Extreme sediment delivery events recorded in the contemporary sediment record of a montane lake, southern Coast Mountains, British Columbia, *Can. J. Earth Sci.*, *43*, 1777–1790, doi:10.1139/E06-056.

Schulz, M., and M. Mudelsee (2002), REDFIT: Estimating red-noise spectra directly from unevenly spaced paleoclimatic time series, *Comput. Geosci.*, *28*, 421–426, doi:10.1016/S0098-3004(01)00044-9.

Selvaraj, K., T. A. C. Chen, and J. Y. Lou (2007), Holocene East Asian monsoon variability: Links to solar and tropical Pacific forcing, *Geophys. Res. Lett.*, *34*, L01703, doi:10.1029/2006GL028155.

Shrestha, A., and R. Kostaschuk (2005), El Niño/Southern Oscillation (ENSO)–related variability in mean-monthly stream flow in Nepal, *J. Hydrol.*, *308*, 33–49, doi:10.1016/j.jhydrol.2004.10.020.

Smith, S. F., R. S. Bradley, and M. B. Abbott (2004), A 300 year record of environmental change from Lake Tuborg, Ellesmere Island, Nunavut, *Can. J. Paleolimnol.*, *32*, 137–148, doi:10.1023/B:JOPL.0000029431.23883.1c.

Sun, Q., G. Chu, J. Liu, and D. Gao (2006), A 150-year record of heavy metals in the varved sediments of Lake Bolterskardet, Svalbard, *Arct. Antarct. Alp. Res.*, *38*, 436–445, doi:10.1657/1523-0430(2006)38[436:AYROHM]2.0.CO;2.

Thompson, L. G., T. Yao, and E. Mosley-Thompson (2000), A high-resolution millennial record of the South Asian monsoon from Himalayan ice cores, *Science*, *289*, 1916–1919, doi:10.1126/science.289.5486.1916.

Tomkins, J. D., S. F. Lamoureux, and D. J. Sauchyn (2008), Reconstruction of climate and glacial history based on a comparison of varve and tree-ring records from Mirror Lake, Northwest Territories, Canada, *Quat. Sci. Rev.*, *27*, 1426–1441, doi:10.1016/j.quascirev.2008.04.012.

Torrence, C., and P. J. Webster (1999), Interdecadal changes in the ENSO-monsoon system, *J. Clim.*, *12*, 2679–2690, doi:10.1175/1520-0442(1999)012<2679:ICITEM>2.0.CO;2.

Wang, N. L., X. Jiang, L. G. Thompson, and M. E. Davis (2007), Accumulation rates over the past 500 years recorded in ice cores from the northern and southern Tibetan Plateau, China, *Arct. Antarct. Alp. Res.*, *39*, 671–677, doi:10.1657/1523-0430(07-507)[WANG]2.0.CO;2.

Wang, X. C., Q. B. Zhang, K. P. Ma, and S. C. Xiao (2008), A tree-ring record of 500-year dry-wet changes in northern Tibet, China, *Holocene*, *18*, 579–588, doi:10.1177/0959683608089212.

Webster, P. J. (1995), The annual cycle and the predictability of the tropical coupled ocean-atmosphere system, *Meteorol. Atmos. Phys.*, *56*, 33–55, doi:10.1007/BF01022520.

Webster, P. J., V. O. Magana, T. N. Palmer, J. Shukla, R. A. Tomas, M. Yanai, and T. Yasunar (1998), Monsoons: Process, predictability, and the prospects for prediction, *J. Geophys. Res.*, *103*, 14,451–14,510, doi:10.1029/97JC02719.

Yao, T., L. G. Thompson, E. Mosley-Thompson, Z. Yang, X. Zhang, and P. Lin (1996), Climatological significance of δ^{18}O in north Tibetan ice cores, *J. Geophys. Res.*, *101*, 29,531–29,537, doi:10.1029/96JD02683.

Yao, T. D., J. C. Pu, Y. Q. Wang, and W. S. Yu (2007), Recent glacial retreat and its impact on hydrological processes on the Tibetan Plateau, China, and surrounding regions, *Arct. Antarct. Alp. Res.*, *39*, 642–650, doi:10.1657/1523-0430(07-510)[YAO]2.0.CO;2.

Zhang, D. Q., D. H. Qin, S. G. Hou, S. C. Kang, and J. W. Ren (2004), Net accumulation rate of the East Rongbuk glacier and Indian summer monsoon rainfall (in Chinese with English abstract), *J. Glaciol. Geocryol.*, *26*, 129–134.

Zhao, H., and G. W. K. Moore (2004), On the relationship between Tibetan snow cover, the Tibetan Plateau monsoon and the Indian summer monsoon, *Geophys. Res. Lett.*, *31*, L14204, doi:10.1029/2004GL020040.

Zhou, A. F., F. H. Chen, M. R. Qiang, M. L. Yang, and J. W. Zhang (2007), The discovery of annually laminated sediments (varves) from shallow Sugan Lake in inland arid China and their paleoclimatic significance, *Sci. China Ser. D*, *50*, 1218–1224, doi:10.1007/s11430-007-0081-1.

Zolitschka, B. (1996), High resolution lacustrine sediments and their potential for paleoclimatic reconstruction, in *Climatic Variations and Forcing Mechanisms of the Last 2000 Years*, edited by P. D. Jones, R. S. Bradley, and J. Jouzel, pp. 453–478, Springer, Berlin.

G. Chu, Q. Liu, X. Wang, and M. Xie, Key Laboratory of Cenozoic Geology and Environment, Institute of Geology and Geophysics, Chinese Academy of Sciences, Beijing 100029, China.

A. Li, H. Wang, F. Yan, K. Yang, and X. Yu, Shanghai Synchrotron Radiation Facility, Shanghai Institute of Applied Physics, Chinese Academy of Sciences, Shanghai 201204, China.

Y. Lin, M. Liu, Q. Sun, and T. Xu, National Research Center of Geoanalysis, Beijing 100037, China.